Analysis and Design of Photovoltaic Pumping System based on Nonlinear Speed Controller

Fouad Zebiri[b], Abdelhalim Kessal[a], Lazhar Rahmani[b], Ali Chebabhi[a,*]

[a]*Faculty of Sciences & Technology, Bordj Bou Arreridj University, Algeria*
[b]*Laboratoire d'automatique, University of Setif 1, Algeria*

Abstract

This paper presents an analysis by which the dynamic performances of a permanent magnet brushless DC (PM-BLDC) motor is controlled through a hysteresis current loop and an outer speed loop with different controllers. The dynamics of the photovoltaic pumping drive system with sliding mode speed controllers are presented. The proposed structure is comprised of a photovoltaic generator associated to a DC-DC converter controlled by fuzzy logic to ensure maximum power point tracking. The PWM signals are generated by the interaction of the motor speed closed-loop system and the current hysteresis. The motor reference current is compared with the motor speed feedback signal. The considered model has been implemented in the Matlab /Simpower environment. The results show the effectiveness of the proposed method in increasing the performance of the water pumping system.

Keywords: Photovoltaic, Permanent magnet brushless DC (PMBLDC) motor, MPPT, Speed control, Fuzzy, Sliding Mode

1. Introduction

The demand for electricity has grown steadily in recent years, driving research into the design and development renewable energy sources such as photovoltaic (PV) [1–3]. Photovoltaic energy is becoming one of the most popular sources since it is clean, inexhaustible and requires little maintenance [4–6].

The utilization of photovoltaic conversion of solar energy to power water pumps is an emerging technology, characterized by gradually declining costs and increasing familiarization with the technology [3, 4]. The main barrier to the use of photovoltaic pumping systems continues to be the high initial cost. The cost of water in these systems is directly related to the cost, efficiency and reliability of the various components and systems involved. While manufacturing techniques have improved, a profitable photovoltaic module is continuously sought. There is a clear need for development towards improved reliability and performance values of subsystem solar pumping to extract the maximum power from the solar generator at all times. Hence, the development of system components has been of interest to many researchers especially in the last ten years [7]. Solar power in Algeria has significant potential. Indeed, the country receives more than 3000 hours of sunshine per year a . The annual average daily solar insolation varies from 5 to 7 KWh/m^2 insofar as the angles of the inclined surfaces are considered optimum [5].

This work proposes an efficient speed controller scheme that can achieve high accuracy and a fast dynamic response of the electrical machine. In order to drive a permanent magnet brushless DC motor (PMBLDC) coupled to a centrifugal pump, an online fuzzy optimization of global efficiency of PV is presented. The PMBLDC motor was introduced mainly for its robustness and relatively low cost [8]. Water discharge depends on the head and speed of the motor, which can be controlled by sliding mode. Therefore, the control parameters include the DC link voltage and the fre-
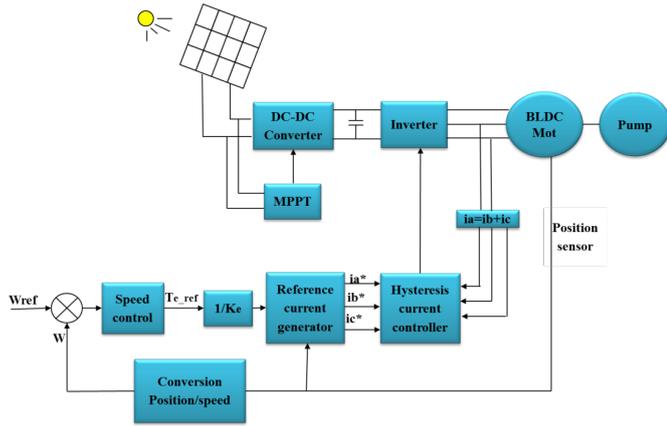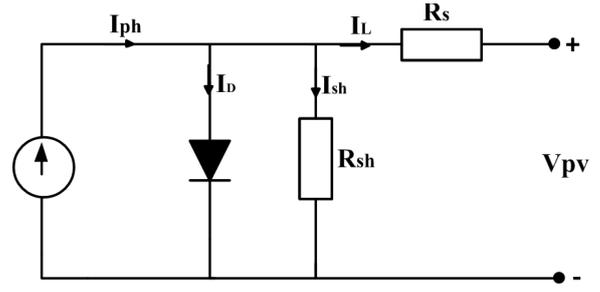

Figure 1: Overall system presentation

Figure 2: Equivalent circuit of PV array

quency of the inverter. In certain cases the pumping head (H) can also be considered as a secondary input variable. The fuzzy optimization procedure, which aims to maximize global efficiency, has led consequently to maximize drive speed and the water discharge rate of the coupled centrifugal pump using variable rotational speed and a modular number of working stages, thus achieving the highest efficiency of the system for all conditions.

This work presents a novel control system for a pumping system fed by a solar system. In order to deal with non linear states a non linear techniques based on fuzzy and sliding mode are applied to improve the performance of the system. This paper is divided into 3 sections, in the first, the various stages of the system are modeled and non linear control algorithms based on fuzzy logic and sliding mode are applied. The simulations of the whole system with applied control laws are presented with appropriate discussions. The paper ends with a conclusion section.

2. System Modeling

The pumping system is an association of a set of inter-connected subsystems, which are: photovoltaic generator, DC-DC converter, PWM voltage source inverter, permanent magnet brushless DC (PMBLDC) motor and the centrifuges pump associated to a repression drain. Fig. 1 shows a schematic block diagram of the system [6, 7, 9].

2.1. PV generator model

The direct conversion of solar energy to electrical power is performed by solar cells. They are often called semiconductor devices and convert sunlight to direct current electricity. Groups of PV cells are electrically configured into modules and arrays. The solar cell may be modeled as current source in parallel with a diode, so shunt and a series resistance are added to the model. The equivalent circuit of the solar cell is shown in Fig.2.

The PV panel is composed of NP parallel modules, each one including a series connected NS photovoltaic cell. The fundamental equation for the PV model is given by Eq. (1) [10]:

$$I_L = I_{ph} - I_D - I_{sh} \tag{1}$$

$$I_L = N_p I_{ph} - N_p I_0 \left\{ \exp \left[\frac{q(U_{pv} + I_L R_s)}{akTN_s} \right] - 1 \right\} - \frac{U_{pv} + I_L}{R_{sh}} \tag{2}$$

where: I_L—PV panel output current; U_{pv}— PV panel output voltage; I_{ph}—generated photocurrent; R_{sh}, R_s—parallel and series resistance, respectively; q—electron charge; k—Boltzmann's constant; a—$p-n$ junction ideality factor; I_0—cell reverse saturation current is related to temperature T as follows:

$$I_0 = I_{0r} \left(\frac{T}{T_r} \right)^3 \exp \left\{ \frac{qE_c}{ka} \left[\frac{1}{T_r} - \frac{1}{T} \right] \right\} \tag{3}$$

where: T, T_r— real and reference temperature, respectively; I_{0r}—reverse saturation current.

Similarly, the photocurrent I_{ph} depends G_n the solar radiation and the cell temperature as follows:

$$I_L = \{ I_{scr} + k_i(T - 298) \} \frac{G_n}{100} \tag{4}$$

where: I_{sc}—short–circuit current; G—solar radiation; k_i—temperature coefficient for short circuit current.

Based on equations (2) to (4), the PV panel can be modeled [3, 11]. Voltage and current of the PV cell depends on the solar radiation and temperature, which
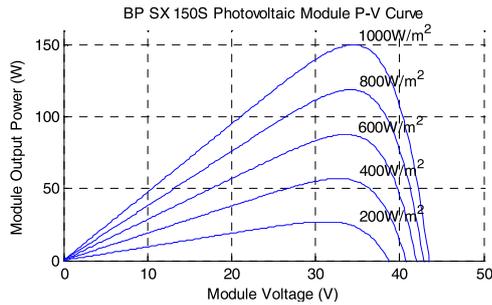
Figure 3: Power curves of BP SX 150S PV module at various temperatures simulated with the MATLAB model
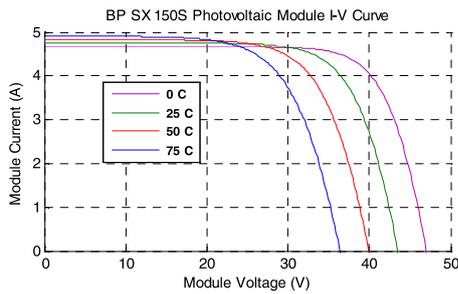

Figure 4: I-V curves of BP SX 150S PV module at various sun radiations simulated with the MATLAB model

varies with the climatic conditions at the particular location. Fig. 3 shows the variation of power with solar radiation [12, 13].

2.2. DC-DC converter

A boost converter can be used to increase voltage magnitude for an inverter circuit and to control MPPT. FLC and pulse width modulation (PWM) method are used to generate a pulse for drive controllable switch. The output voltage of the boost converter can be calculated from:
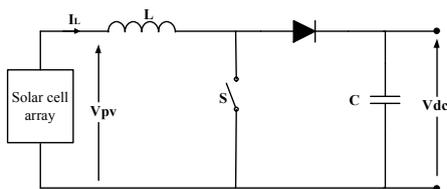
$$V_{pv} = \frac{1}{1-D} V_{dc} \tag{5}$$
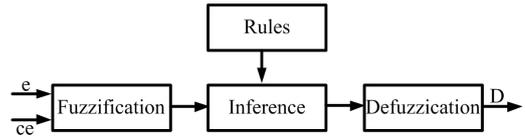

Figure 5: Basic circuit of the boost chopper

Figure 6: Diagram of fuzzy logic controller

Table 1: Fuzzy rules

$\triangle e \downarrow / e \rightarrow$	NB	NS	Z	PS	PB
NB	Z	Z	PS	NS	NB
NS	Z	Z	Z	NS	NB
Z	PB	PS	Z	NS	NB
PS	PB	PS	Z	Z	Z
PB	PB	PS	NS	Z	Z

2.3. Fuzzy Logic MPPT tracking controller

This section presents a procedure for fuzzy logic controller design for a MPPT system using Matlab Fuzzy Logic Toolbox, which is an effective tool for the conception and design of fuzzy systems. There are several ways to design fuzzy logic controllers. A simple step by step design procedure, based on Mamdani linguistic models, is presented in this section [14–16].

The proposed FL MPPT Controller, shown in Fig. 6, has two inputs and one output. The two FLC input variables are: error (e) and change of error (△e) at sampled times k defined by:

$$e(k) = \frac{p(k) - p(k-1)}{v(k) - v(k-1)} \tag{6}$$

$$\Delta e(k) = e(k) - e(k-1) \tag{7}$$

The control rules are indicated in Table 1 with (e) and (△e) as inputs and (D: Duty cycle) as output.

The irradiance and temperature profiles are shown in Fig. 7. Irradiance levels can experience instantaneous changes because of shading or accumulated dust. The intervals of change are 0 s to 1 s, 1 s to 2 s, 2 s to 3 s and 3 s to 4 s, where the levels of temperature and irradiance are 1 kW/m² @ 25°C, 0.3 kW/m² @ 25°C, 0.5 kW/m² @ 50°C and 0.8 kW/m² @ 25°C respectively.

At these conditions the fuzzy logic MPPT response is shown in Figs. 8. As can be seen, the FLC algorithm converges in smaller times. Reactions of fuzzy logic
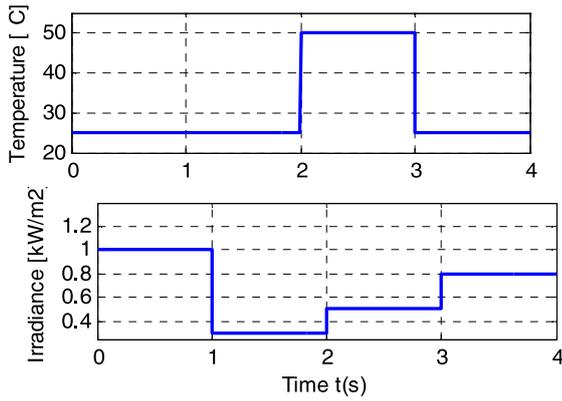
Figure 7: Irradiance and temperature profiles

controllers have shown their robustness under rapid changing conditions and their adaptability to nonlinearities. All quantities (speed and power of GPV) stabilize after a response time △t= 0.15s after each irradiance level applied. Thus it can be seen that there are oscillation magnitudes for different conditions because of the MPPT technique and chopping frequency.

2.4. Permanent magnet Brushless DC motor model

DC motors have been gradually replaced by BLDC motors in recent years, because industrial applications require more powerful, compact actuators. Flexibility of control, long life due to the absence of mechanical commutation and low acoustic noise are the main advantages of this type of motor [17].

The coupled circuit equations of the stator windings in terms of motor electrical constants are [18, 19]:

$$
\begin{bmatrix} V_{as} - v_n \\ V_{bs} - v_n \\ V_{cs} - v_n \end{bmatrix} = \begin{bmatrix} R_s & 0 & 0 \\ 0 & R_s & 0 \\ 0 & 0 & R_s \end{bmatrix} \begin{bmatrix} I_a \\ I_b \\ I_c \end{bmatrix} \\ + p \begin{bmatrix} L & M & M \\ M & L & M \\ M & M & L \end{bmatrix} \begin{bmatrix} I_a \\ I_b \\ I_c \end{bmatrix} + \begin{bmatrix} E_a \\ E_b \\ E_c \end{bmatrix} \tag{8}
$$

where: R_s—Stator resistance per phase; I_a, I_b, and I_c—Stator phase currents; p—d/dt is the time derivative operator; E_a, E_b, and E_c—represent the back emfs in the respective phases in (8); v_n—is the neutral point node voltage given by:

$$
v_n = \frac{1}{3} [V_{as} + V_{bs} + V_{cs}] - \sum BE \tag{9}
$$

$\sum BEMFs$ means summing up the individual phase emfs on an instant to instant basis.

The induced emfs are all assumed to be trapezoidal, whose peak value is given by:
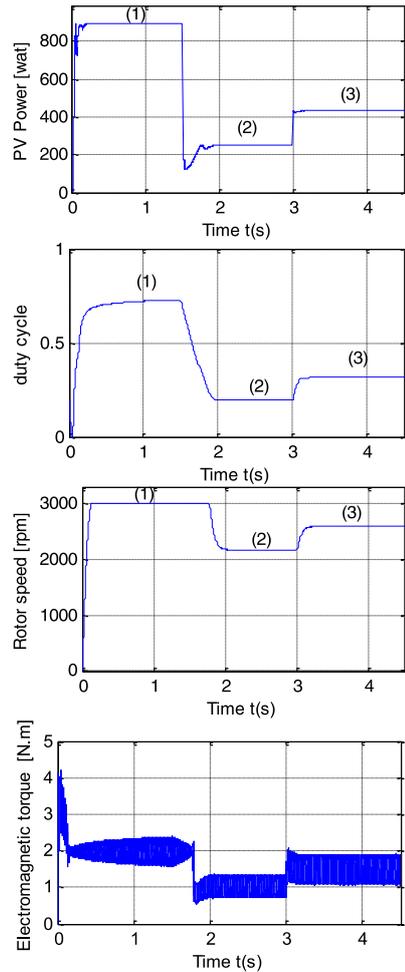

Figure 8: Responses results of MPPT-FLC

$$
E_p = \lambda \omega \tag{10}
$$

where: ω—electrical angular speed in rad/sec; λ—total flux linkage given;

By simplifying (8):

$$
\begin{bmatrix} V_{as} - v_n \\ V_{bs} - v_n \\ V_{cs} - v_n \end{bmatrix} = R_s \begin{bmatrix} 1 & 0 & 0 \\ 0 & 1 & 0 \\ 0 & 0 & 1 \end{bmatrix} \begin{bmatrix} I_a \\ I_b \\ I_c \end{bmatrix} \\ + p \begin{bmatrix} L-M & 0 & 0 \\ 0 & L-M & 0 \\ 0 & 0 & L-M \end{bmatrix} \begin{bmatrix} I_a \\ I_b \\ I_c \end{bmatrix} + \begin{bmatrix} E_a \\ E_b \\ E_c \end{bmatrix} \tag{11}
$$

The mechanical part is expressed by:

$$
\frac{d\omega}{dt} = \frac{1}{j} (-B\omega + T_e - T_l) \tag{12}
$$

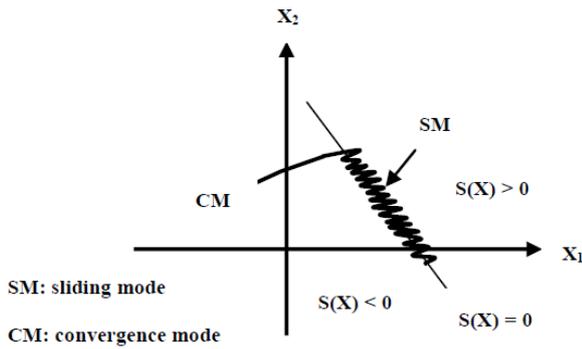where: T_l load torque; J—moment of inertia; B—friction coefficient.

Figure 9: Trajectory mode in the phase plane

2.5. Speed control

2.5.1. Sliding mode control

Sliding mode control has been very successful in recent years. This is due to the simplicity of implementation and robustness with respect to uncertainties in the system and external disturbances vitiating the process. Sliding Mode control aims to reduce the state trajectory to the sliding surface and to develop it with a certain dynamic to the point of equilibrium [17, 18, 20]. This trajectory consists of three parts:

Choice of the switching surface

It is determined on the basis of the system and the desired performance. In general, consider the system described by the following non-linear state-space representation:

$$\begin{cases} x^n = f(x,t) + g(x,t)u \\ x \in R^n, u \in R^m \end{cases} \qquad (13)$$

where $x = \left[x, \dot{x}, \ddot{x} ... x^{n-1} \right]^T$ is the state vector, u is the control input, $f(x,t)$ and $g(x,t)$ are non–linear functions continuous and uncertain assumed bounded. The general form equations for the sliding surface given by "JJ Slotinie":

$$\begin{cases} S(x) = (\frac{d}{dt} + \lambda)^{r-1} e(x), \qquad \lambda > 0 \\ e(x) = x_{ref} - x \end{cases} \qquad (14)$$

Convergence condition

The convergence condition makes it possible for the dynamic system to converge to the sliding surfaces. It is defined by the equation of Lyapunov [21, 22] which makes the surface attractive and invariant:

$$\dot{S}(x).S(x) < 0 \qquad (15)$$

Determining the law of control

The control algorithm is defined by the relationship:

$$u = u_{eq} + u_n \qquad (16)$$

Where u_{eq} size the equivalent command and u_n size the discontinuous command.

The equivalent component (u_{eq}) can be interpreted as the average value modulated,

$$S(x) = 0 \Rightarrow \dot{S}(x) = 0 \qquad (17)$$

The Nonlinear component (u_n) is determined to secure the attractiveness of the variable to be controlled to the sliding surface and satisfy the convergence condition.

$$\dot{S}(x).S(x) < 0 \qquad (18)$$

The simplest solution satisfying this condition takes the form:

$$u_n = K. \sin(S(x)) \qquad (19)$$

Speed control of BLDC motor by sliding mode

The mathematical model that governs the mechanical system of the machine is defined by:

$$J(\frac{d\omega}{dt}) + B\omega = T_e - T_l \qquad (20)$$

We consider as state variable x1, x2, such that:

$$\begin{cases} x_1 = \omega_{ref} - \omega \\ x_2 = \dot{x}_1 \\ \frac{dx_2}{dt} = \frac{B}{J}x_2 - \frac{1}{J}u \end{cases} \qquad (21)$$

where: $u = \frac{dT_e}{dt}$—is the control variable.

The form of the control variable used in the sliding trajectory is given by the following relationship [21]:

$$U = A_1 x_1 + A_2 x_2 \qquad (22)$$

where: x_1, x_2—error and its derivation successively; A_1, A_2: Control parameters (control gains).

$$A_1 = \begin{cases} \alpha_1 & for & S.x_1 > 0 \\ \beta_1 & for & S.x_1 < 0 \end{cases}$$
$$A_2 = \begin{cases} \chi_1 & for & S.x_2 > 0 \\ \delta_1 & for & S.x_2 < 0 \end{cases}$$

To determine the controller parameters, we apply the convergence conditions (18).
Where S(x) is the sliding surface represented by the following equation:
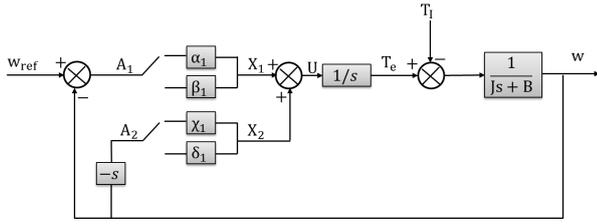
Figure 10: Simplified model of the drive system

$$S(x) = \lambda x_1 + x_2 \qquad (23)$$

We obtained:

$$\frac{dS(x)}{dt} = \lambda \frac{dx_1}{dt} + \frac{dx_2}{dt} = \lambda x_2 + \frac{B}{J} x_2 - \frac{1}{J} u \qquad (24)$$

$$S(x)\frac{dS(x)}{dt} = (\lambda x + x_2)((\lambda + \frac{B}{J} - \frac{1}{J}A_2)x_2 + \frac{1}{J}A_1 x_1) \qquad (25)$$

Then, the convergence condition is written as

$$S(x)\frac{dS(x)}{dt} = (\lambda x + x_2)((\lambda + \frac{B}{J} - \frac{1}{J}A_2)x_2 + \frac{1}{J}A_1 x_1) < 0 \qquad (26)$$

The conditions are:

$$\begin{cases} \lambda x_1 + x_2 > 0 \\ (\lambda + \frac{B}{J} - \frac{1}{J}A_2)x_2 + \frac{1}{J}A_2 x_2 < 0 \end{cases} \qquad (27)$$

Or,

$$\begin{cases} \lambda x_1 + x_2 < 0 \\ (\lambda + \frac{B}{J} - \frac{1}{J}A_2)x_2 + \frac{1}{J}A_2 x_2 > 0 \end{cases} \qquad (28)$$

$\alpha_1, \beta_1, \chi_1, \delta_1$: are obtained by considering ($x_1 > 0$, $x_2 < 0$).

1st case:

$$\lambda x_1 + x_2 > 0 \text{ Then } \begin{cases} S.x_1 > 0 \Rightarrow A_1 = \alpha_1 \\ S.x_2 < 0 \Rightarrow A_2 = \delta_1 \end{cases}$$

$$(\lambda + \frac{B}{J} - \frac{1}{J}A2)x2 + \frac{1}{J}A2x2 < 0$$

$$\text{Then } \begin{cases} \lambda + \frac{B}{J} - \frac{1}{J}\delta_1 > 0 \Rightarrow \delta_1 < J\lambda + B \\ -\frac{1}{J}\alpha_1 < 0 \Rightarrow \alpha_1 > 0 \end{cases}$$

2nd case:

$$\lambda x_1 + x_2 < 0 \text{ Then } \begin{cases} S.x_1 > 0 \Rightarrow A_1 = \beta_1 \\ S.x_2 < 0 \Rightarrow A_2 = \chi_1 \end{cases}$$

$$(\lambda + \frac{B}{J} - \frac{1}{J}A_2)x_2 + \frac{1}{J}A_1 x_1 > 0 \text{ Then}$$
$$\begin{cases} \lambda + \frac{B}{J} - \frac{1}{J}x_1 < 0 \Rightarrow \chi_1 > J\lambda + B \\ -\frac{1}{J}\beta_1 > 0 \Rightarrow \beta_1 < 0 \end{cases}$$
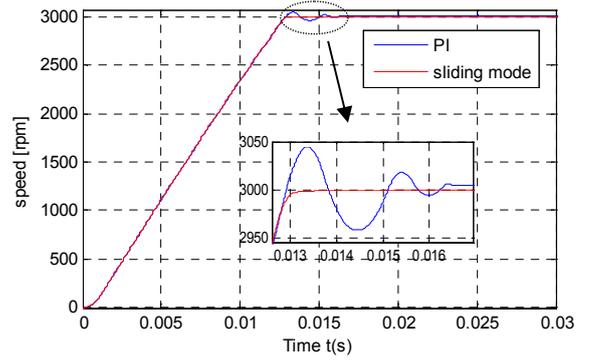

Figure 11: Comparative response of the speed control using sliding mode and PI controllers

With a resistant torque and positive speed error control, the control gains are given by:

$$\begin{cases} x_1 > J\lambda + B > \delta_1 \\ \beta_1 < 0 < \alpha_1 \end{cases} \qquad (29)$$

Fig. 11 shows the response speed using sliding mode and PI controllers.

2.6. The pump

The centrifugal pump torque T_I is assumed to be proportional to the square of the rotor speed.

$$T_{lc} = K_{pump}\omega^2 \qquad (30)$$

where: K_{pump} is the constant for a given pump.

The flow head characteristic of a centrifugal pump is given by the following expression:

$$H_n = a_1 W^2 + a_2 WQ + a_3 Q^3 \qquad (31)$$

where: a_1, a_2 and a_3 are geometric parameters of the pump; Q—Flow rate of the pump (m^3/h); H—Total height (m); W—The motor speed.

3. Simulation of the pumping system under PV generator

In this section, the results of simulations of the PV water pumping system are presented. Fig. 12 presents the simulation diagram of the considered system. The system was simulated with the hysteresis current controller and sliding mode speed regulator.

The simulation results given by Figs. 13 illustrate the waveforms of speed, stator current, EMF, electromagnetic torque of the BLDC motor and the power delivered by the GPV. We note the rotor speed value. It
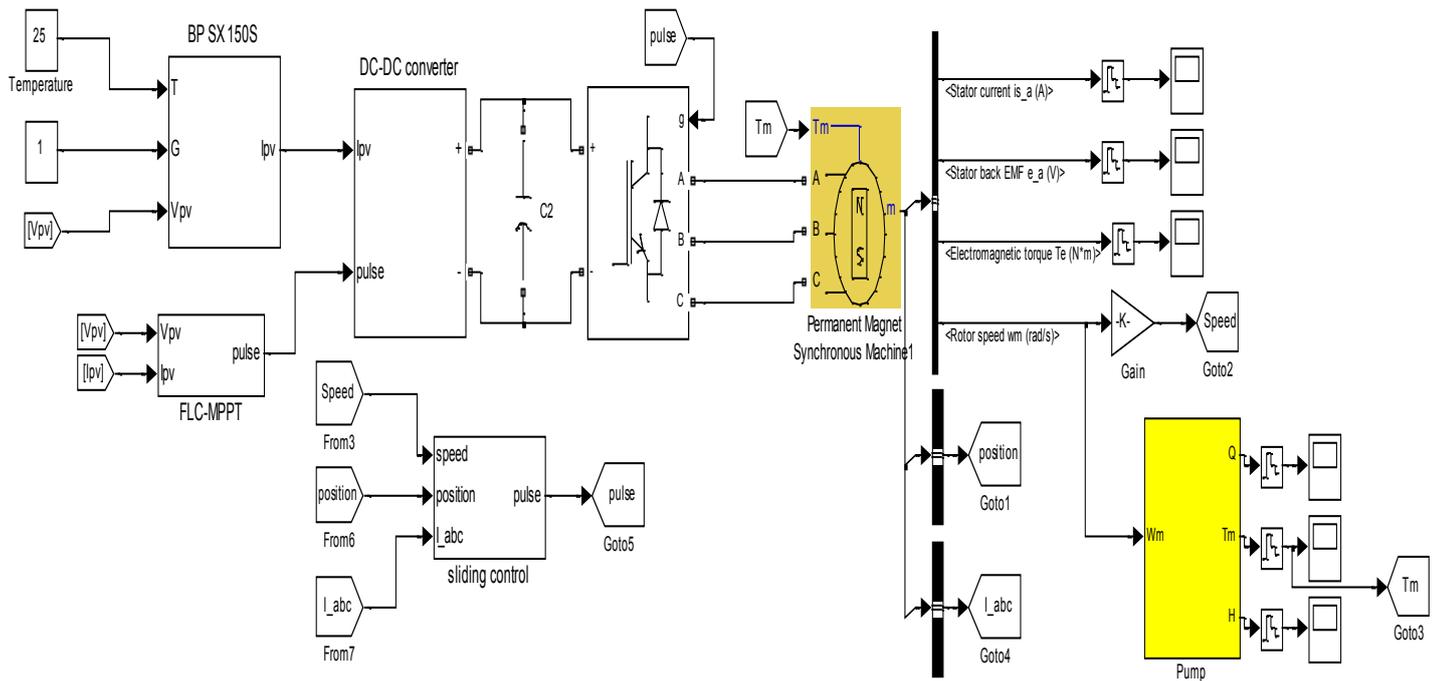
Figure 12: Simulink model global system

is noted that: ω_r=3,000 rpm and the electromagnetic torque T_e = 2 N·m, K_e (gain of error) and K_{ce} (gain of variation of error) are chosen to allow the sensitivity of the fuzzy controller to change without changing its structure. $K_{ce} = 1,000$, $K_e = 0.01$.

We apply, every 1.5 s, three levels of irradiance, so that G=1,000 W/m, G=300 W/m, and G=500 W/m are obtained successively with constant temperature T=25°C, according to the results simulation shown in Fig. 13. First level of irradiance is G=1,000 W/m^2 (Fig. 13a) where the value of the power Maximum GPV is 892.8 W corresponding to an optimum speed of 3,000 rpm (Fig. 13c). Then the stator current varies around a reference value of 4.2 A (Fig. 14a).

For lower irradiance 300 W/m, there is a power decrease in the maximum power up to 250 W, the same speed and stator current BLDC decreased by approximately 830 rmp and 2.4 A, which corresponds to percentages of 27.7%, 54% and 28% respectively for speed, stator current and power.

There is another sharp increase in irradiance of 500 W/m^2, which gives a maximum power of 431.5 W, similarly, the speed and stator current will have values of about 2,593 rmp and 3 A respectively. We therefore deduce a gain of 51.7% in power, 28.5% to stator current and 13.6% for speed.

4. Conclusion

In this work, the objective was to control the voltage solar panel to obtain the maximum power possible from a photovoltaic generator, regardless of the solar insolation and temperature conditions. Fuzzy logic controllers can provide a more effective order than traditional controllers for nonlinear systems, because there is more flexibility. Control strategies are presented to regulate the flow of water from a based PV pumping system BLDC water and control their speed from a sliding mode controller. Comparisons of simulation results demonstrate that the performance of the sliding mode controller is satisfactory under steady state as well as dynamic conditions.
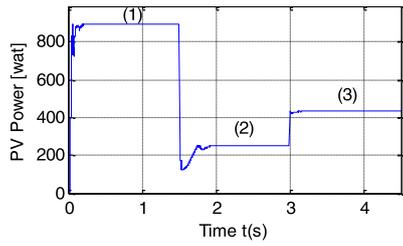
Acknowledgments

References

[1] C.-H. Lin, C.-H. Huang, Y.-C. Du, J.-L. Chen, Maximum photovoltaic power tracking for the pv array using the fractional-

order incremental conductance method, Applied Energy 88 (12) (2011) 4840–4847.

[2] A. El Shahat, Pv module optimum operation modeling, Journal of Power technologies 94 (1) (2014) 50.

[3] A. Betka, A. Moussi, Maximum efficiency of an induction motor fed by a photovoltaic source, Larhyss Journal (02) (2003) 151–162.

[4] P. Bajpai, V. Dash, Hybrid renewable energy systems for power generation in stand-alone applications: a review, Renewable and Sustainable Energy Reviews 16 (5) (2012) 2926–2939.

[5] A. Hamidat, A. H. Arab, M. Boukadoum, Performances et coûts des systèmes de pompage pv en algérie, Rev. Energ. Ren 8 (2005) 157–166.

[6] A. Terki, A. Moussi, A. Betka, N. Terki, An improved efficiency of fuzzy logic control of pmbldc for pv pumping system, Applied Mathematical Modelling 36 (3) (2012) 934–944.

[7] A. Betka, A. Moussi, Performance optimization of a photovoltaic induction motor pumping system, Renewable energy 29 (14) (2004) 2167–2181.

[8] I. Odeh, Y. Yohanis, B. Norton, Influence of pumping head, insolation and pv array size on pv water pumping system performance, Solar energy 80 (1) (2006) 51–64.

[9] A. Betka, A. Attali, Optimization of a photovoltaic pumping system based on the optimal control theory, Solar Energy 84 (7) (2010) 1273–1283.

[10] A. Tofighi, Performance evaluation of pv module by dynamic thermal model, Journal of Power Technologies 93 (2) (2013) 111.

[11] K. Hussein, I. Muta, T. Hoshino, M. Osakada, Maximum photovoltaic power tracking: an algorithm for rapidly changing atmospheric conditions, in: Generation, Transmission and Distribution, IEE Proceedings-, Vol. 142, IET, 1995, pp. 59–64.

[12] BP Solar BP SX150-150W Multi-crystalline Photovoltaic Module Datasheet, 2001.

[13] M. Gupta, R. Jain, A. Goswami, Design and simulation of photovoltaic system using advance mppt, International Journal of Advance Technology & Engg. Research 2 (2012) 73–76.

[14] I. Purnama, Y.-K. Lo, H.-J. Chiu, A fuzzy control maximum power point tracking photovoltaic system, in: fuzzy systems (FUZZ), 2011 IEEE international conference on, IEEE, 2011, pp. 2432–2439.

[15] F. Aashoor, F. Robinson, Maximum power point tracking of photovoltaic water pumping system using fuzzy logic controller, in: Power Engineering Conference (UPEC), 2013 48th International Universities', IEEE, 2013, pp. 1–5.

[16] A. Kerboua, Hybrid fuzzy sliding mode control of a doubly-fed induction generator speed in wind turbines, Journal of Power Technologies 95 (2) (2015) 126.

[17] A. Terki: controle flou-genetique hybride d'un moteur BLDC dans un système de pompage photovoltaique. (2011) Ph.D Thesis, university of Biskra, Algérie.

[18] C. Umayal, D. S. Devi, Modeling and simulation of pfc sepic converter fed pmbldc drive for mining application, International Journal of Advanced Trends in Computer Science and Engineering 2 (2) 203–208.

[19] C. Navaneethakkannan, M. Sudha, Minimum rule based pid sliding mode fuzzy control techniques for brushless dc drives, International Journal of Advances in Engineering Technology 4 (2).

[20] J.-J. E. Slotine, Sliding controller design for non-linear systems, International Journal of control 40 (2) (1984) 421–434.

[21] V. I. Utkin, Sliding mode control design principles and applications to electric drives, Industrial Electronics, IEEE Transactions on 40 (1) (1993) 23–36.

[22] V. I. Utkin, Variable structure systems with sliding modes, IEEE Transactions on Industrial Informatics (2).
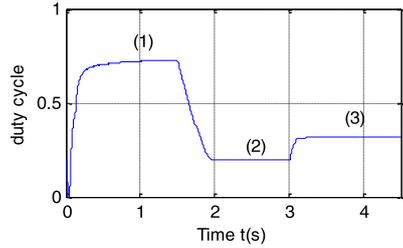
Appendix A

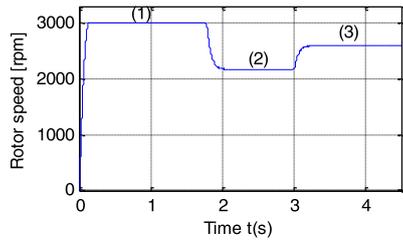The PV generator, motor and pump used in this study have the following parameters:

1. PV generator Modules BP SX 150S
2. Maximum Power (P_{max}) 150W
3. Voltage at Pmax (V_{mp}) 34.5V
4. Current at Pmax (I_{mp}) 4.35A
5. Open-circuit voltage (V_{oc}) 43.5V
6. Short-circuit current (I_{sc}) 4.75A
7. Brushless DC motor
8. Rated power 690W
9. Rated speed 3000 rev/min
10. Rated voltage 200–220 V
11. Rated current 4.8 A
12. Per phase resistance 1.4 Ω
13. Per phase inductance 5mH
14. Poles number 6
15. E.m.f constant 0.47
16. Centrifugal pump
17. Rated speed 3840 rev/min
18. Rated power 521W
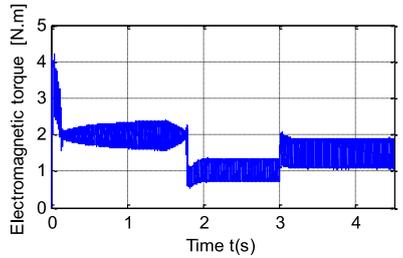19. a_1=4.8e-4, a_2 = -1e^{-10} and a_3= -8e^{-3}

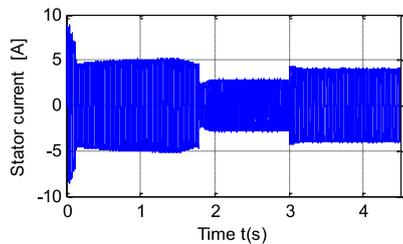(a) Speed response of PV pumping system

(b) Duty cycle response of PV pumping system

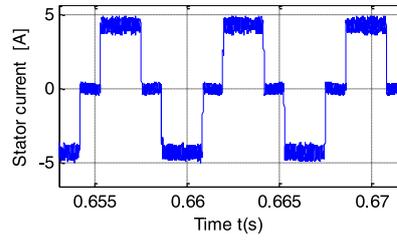(c) Speed response of PV pumping system
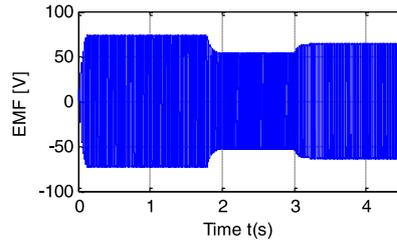

(d) Torque response of PV pumping system
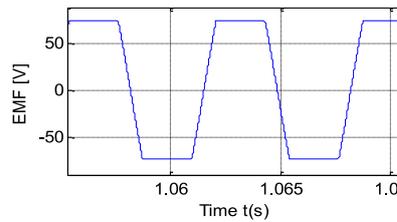

(e) Phase 'a' Current response

Figure 13: Simulation results for different sizes of photovoltaic pumping system (T = 25 ℃). (1) G = 1,000 W/m², (2) G = 300 W/m² and (3) G = 500 W/m²
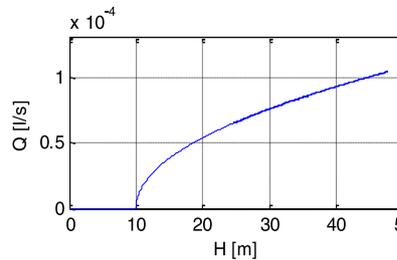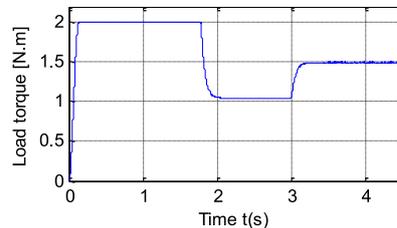

(a) One period of current

(b) Back-EMF

(c) One period of EMF

(d) Variation in the head and flow of PV pumping system

(e) Load torque of PV pumping system

Figure 14: Simulation results for different sizes of photovoltaic pumping system (T = 25 ℃). (1) G = 1,000 W/m², (2) G = 300 W/m² and (3) G = 500 W/m²